SCALING OF ADULT TO CHILD RESPONSES APPLIED TO THE THORAX

J.G.M. Thunnissen, R. Happee, P. Eummelen and M.C. Beusenberg
TNO Crash-Safety Research Centre
P.O. Box 6033
2600 JA Delft
The Netherlands

ABSTRACT

The TNO Crash-Safety Research Centre started a research programme to establish sets of requirements for basic child dummy design characteristics. However, there is only very limited data available on child responses to impact loading and, therefore, most of the response corridors were obtained by scaling the responses of adults. In previous studies, the "Kroell thoracic response corridors" were scaled on the basis of the masses and the rib cage stiffness only. Scaling by this method assumes that the corridor shape is similar and, therefore, implicitly assumes that the thoracic damping of adults is equivalent to that of children. In the present paper a general scaling method is presented and applied to Lobdell's mathematical thoracic response model to predict the thoracic response of children. To derive the scaled thoracic response of a child, the parameters of the model are scaled while using scaling procedures for mass, thoracic stiffness and damping. The thoracic response of the scaled Lobdell model is compared with the scaled "Kroell thoracic response corridors". Even with uncertainties, such as the high dynamic stiffness of the Lobdell model and the current lack of child Post Mortem Human Subject validations, it is believed that a more realistic child thoracic response is derived.

INTRODUCTION

The evaluation of the effectiveness of child protection systems is substantially influenced by the biofidelity of the manikin used in crash-tests. Already in the late sixties, the TNO Crash-Safety Research Centre had developed a series of child manikins, also known as the TNO P-dummies, for the evaluation of Child Restraint Systems (CRS). The developments in crash safety research, the review of ECE R.44 [1]†, the potential upgrading of US Federal Standard on CRS [2] and product enhancements have indicated the need for a review on child dummy design [3],[4]. A research programme was therefore started to establish sets of requirements for basic child dummy design characteristics. To obtain biofidelic child dummy characteristics, impact responses of various parts should be established. These responses can be derived from Post Mortem Human Subjects (PMHS) tests and from volunteer tests. However, at the present time there is only very limited child response data available [5],[6],[7]. It was therefore decided to derive the thoracic responses of children by scaling average normalized adult thoracic responses.

In biomechanics, scaling is a mathematical technique to derive response characteristics or tolerance levels for a specific population based on knowledge of the responses of a different population. Most of the scaling methods currently used, derive the differences in overall stiffness of a certain body part only on the basis of anthropometric differences of this part or the whole body [8],[9]. This approach ignores the fact that there are other differences between these populations which will influence the overall stiffness of a body region. These differences are not only caused by different material properties but also by different functional anatomical aspects [10]. Summarising the results of thoracic impactor tests, anthropometric studies [11] and results from mathematical models studies [9],[12],[13],[14],[15], the thoracic stiffness of a human subject depends upon the integral effect of the following aspects:

† Numbers in parentheses designate references at the end of the paper.

- the dynamic and static constitutive properties of bone and cartilage,
- the geometry of the rib cage and the spine,
- the cross-sectional properties of the bony structures,
- the connection between the rib cage and the sternum, and the rib cage and the spine,
- the dynamic and static stiffness of the internal organs (lungs and heart) and
- the mechanical skin properties.

The objective of this paper is to define a general scaling method which includes these aspects. This scaling method will be applied to the parameters of Lobdell's mathematical thoracic response model [15] in order to predict the thoracic impact response of children at 18 months. This method is called "the model-based scaling method". For comparison with conventional scaling methods, the scaled model response will be compared with "Kroell thoracic response corridors", scaled with Mertz' scaling method [8] also to an age of 18 months. As a basis for both scaling methods a description of the mathematical thoracic response model is first provided.

MODELLING THE THORACIC RESPONSE

A number of chest impact experiments have been conducted using Post Mortem Human Subjects (PMHS), volunteers and animals as test subjects. Kroell et al. (ref. [16],[17]) investigated the effects of impact conditions on the force skeletal-deflection relationship of the human thorax. It was found that in high velocity, low impactor mass cases, the peak force occurred almost immediately after the initial contact of the impactor, the duration of the impulse was relatively short and the impact momentum very low. In contrast, the high impactor mass, low velocity cases produced greater momentum and longer impulse duration.

The effect of muscle tension on the thoracic stiffness was presented by Lobdell et al. [15]. Typical force deflection curves were obtained from volunteers under quasi-static loading conditions. The results showed that the thoracic stiffness was higher under tensioned conditions when compared with the relaxed conditions. The response curves corrected for muscle tension are illustrated in Figure 1 by the solid lines. The curves are based on two different combinations of impactor mass and velocity, see also Table 1. The thin solid line denotes the thoracic response while using an impactor mass of 19.5 kg while the thick solid line denotes the response when using an impactor mass of 23.1 kg. The impactor energy of the "low velocity-low mass" impact is approximately half the impactor energy of the "high velocity-high mass". The dotted lines in this figure are the recommended "Kroell thoracic response corridors" based on these two different impactor conditions [15].

Lobdell et al. [15] used a lumped mass model to describe blunt frontal thoracic impactor tests; the model is illustrated in Figure 2. Lobdell estimated a number of parameter values directly from the PMHS impactor tests and used arbitrary values for the remaining parameters. Depending on the results of the model, parameter values were modified and the response was evaluated. This iterative procedure was continued until the impact response of the system satisfied the "Kroell thoracic response corridors". The results obtained by Neathery and Lobdell [19] illustrated that the response of the Lobdell model without the visco-elastic element (kv_{23} and cv_{23}) still meets the "Kroell thoracic response corridors". Therefore they suggested removing the visco-elastic element.

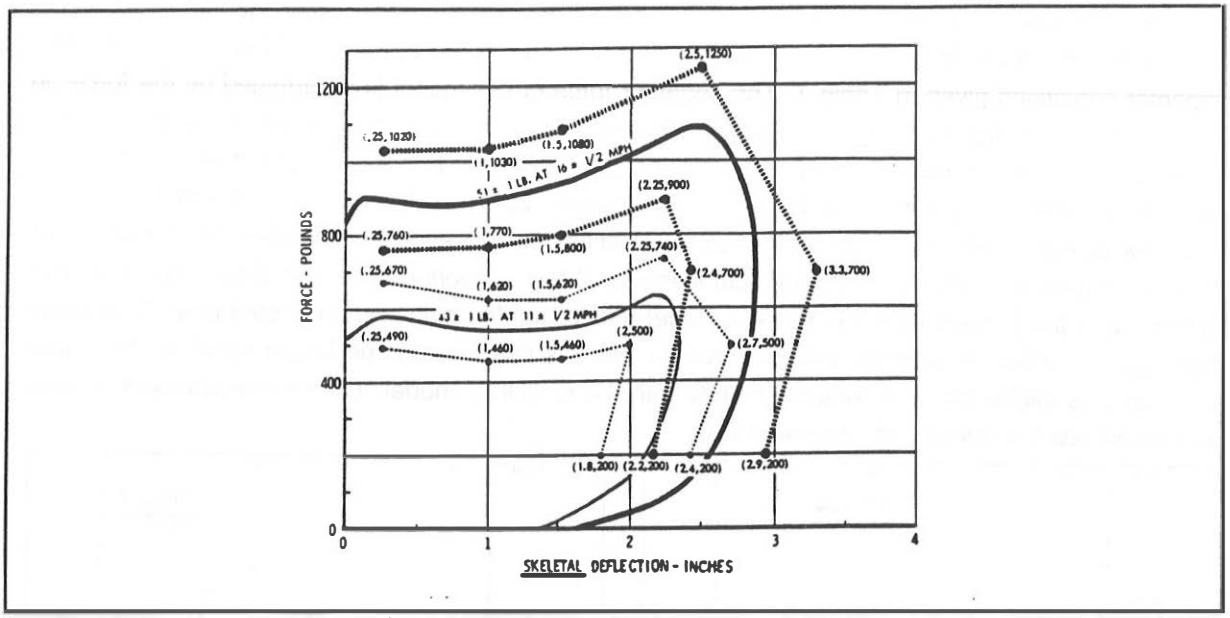

Figure 1 Averaged, corrected force-skeletal deflection curves (solid lines) and "Kroell thoracic response corridors" (dotted lines). From [15].

Table 1 The two thoracic impactor conditions used for the corrected "Kroell thoracic response corridors".

Condition, see also figure 1	Impactor Velocity [m.s^{-1}]	Impactor mass [kg]	Impactor energy [J]
Low velocity (thin line)	4.8 ± 0.2	19.5 ± 0.45	201.5 - 249.4
High velocity (thick line)	7.1 ± 0.2	23.1 ± 0.45	539.2 - 627.5

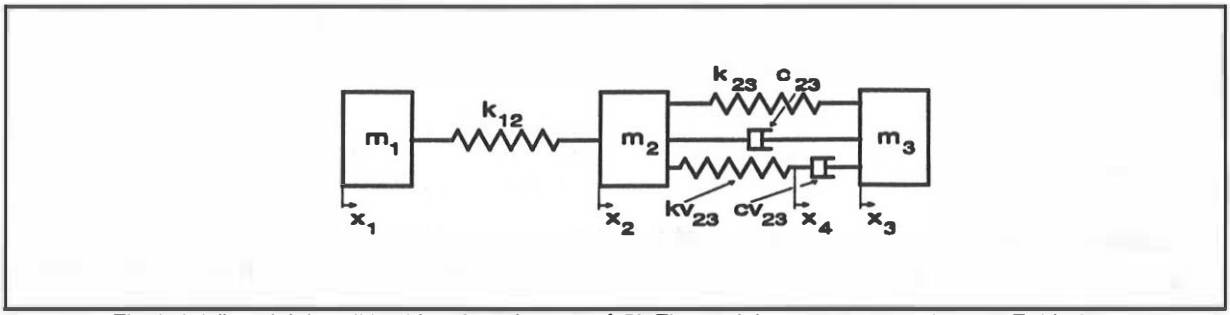

Figure 2 The Lobdell model describing blunt frontal impacts [15]. The model parameters are shown in Table 2.

Table 2 The model parameters as defined by Lobdell et al. [15].

Parameters	Description	Values	
m_1, v_1	impactor mass, impactor velocity	low velocity conditions high velocity conditions	19.5 kg, 4.92 m.s^{-1} 23.1 kg, 7.15 m.s^{-1}
m_2	sternal effective mass	0.45 kg	
m_3	vertebral effective mass	27.2 kg	
k_{12}	stiffness of soft tissue between sternum and impactor	281 kN.m^{-1}	
k_{23}	rib cage stiffness	primary spring stiffness secondary spring stiffness transition point	26.3 kN.m^{-1} 78.8 kN.m^{-1} 31.8 mm
c_{23}	thorax damping	compression decompression	0.525 kN.s.m^{-1} 1.23 kN.s.m^{-1}
kv_{23}, cv_{23}	visco-elastic behaviour of thorax	13.2 kN.m^{-1}, 0.18 kN.s.m^{-1}	

The reconstructed adult force skeletal-deflection curves of the original [15] and the simplified model (without the visco-elastic element kv_{23} and cv_{23}) [19] are shown in Figure 3 and Figure 4 for the two impactor conditions given in Table 1. The impactor force of the model is determined by the force on m_1, which equals the force on spring k_{12}. The skeletal deflection is determined by the relative displacement between m_2 and m_3. The figures indicate that there are only small differences between the original and the simplified model. It seems however that the visco-elastic element flattens the mid-area of the curve by introducing a non-linear stiffness. However, both models meet the "Kroell thoracic response corridors". Secondly, considering all four response curves, it should be taken into account that the Lobdell model is tuned to meet the "Kroell thoracic response corridors". This could imply that for different impactor velocities and/or masses the model is no longer valid. In this paper this aspect is evaluated by a sensitivity study with the simplified model. The simplified model is used here to reduce the number of parameters.

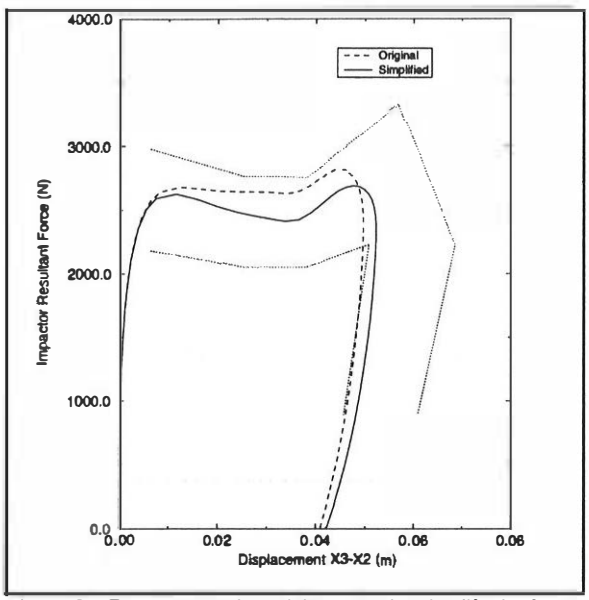

Figure 3 Reconstructed original and simplified force-deflection curves with Kroell corridors (dotted lines), v_{imp} 4.92 m/s and m_{imp} 19.5 kg.

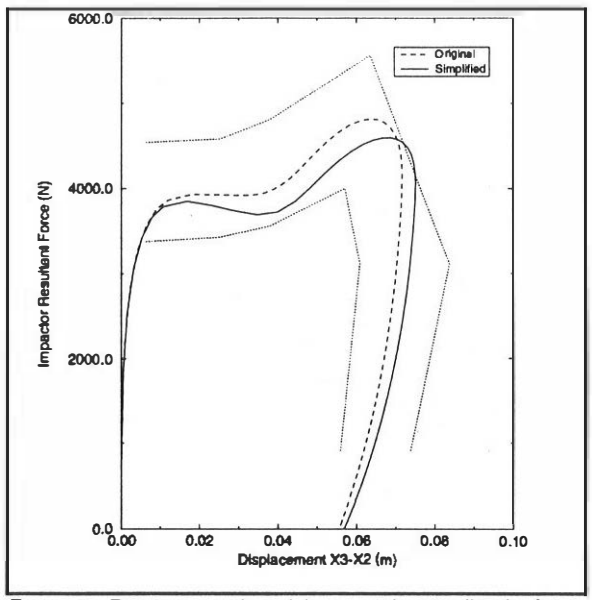

Figure 4 Reconstructed original and simplified force-deflection curves with Kroell corridors (dotted lines), v_{imp} 7.15 m/s and m_{imp} 23.1 kg.

By quantifying certain characteristic points of the impact response curves (Figure 5), the results of parameter permutations are summarised in Table 3; more details are provided in annex A. Table 3 shows that the response is more or less sensitive to all parameters. This table indicates the sensitivity of a single parameter within an arbitrary, but realistic, range. Combinatoric permutations are not made as this will need complex multi-variational statistical analyses, which are beyond the scope of this project. It is expected is that due to the non-linearity of the system, interaction between the parameters may influence the thoracic impact response. However, Lobdell chose most of his parameters separately from the other parameters and estimated only the linear damping coefficient c_{23}. Therefore, within a small range, a linear response can be expected. The influence of the damping factor is large, as illustrated in Figure A.5 and Figure A.6 for compression and decompression respectively.

The results confirm that the Lobdell model has been tuned by the damping coefficient to meet the "Kroell thoracic response corridors", even in such a way that the visco-elastic element can be removed without any significance and the sensitivity of the (static) elastic component is not as large as expected. This could imply that the dynamic stiffness caused by the damper is overestimated and this could also explain the large response sensitivity of the damper coefficient. However, when reducing the thoracic stiffness by 50 percent, it is not possible to derive a damping coefficient to meet the "Kroell thoracic response corridors". This means that the current damping coefficient

represents a realistic amount of internal damping. On the other hand, considering the large sensitivity of the damping parameter while assuming only linear damping could mean that the model is indeed not valid for other impact conditions. A more detailed study of this subject will provide more information but is beyond the scope of this paper.

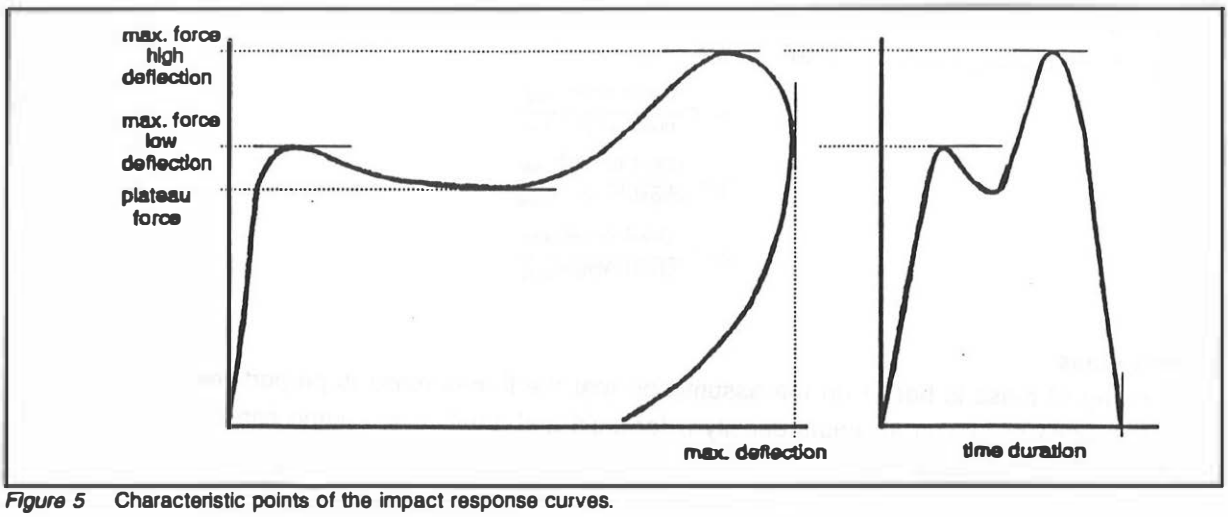

Figure 5 Characteristic points of the impact response curves.

Table 3 Summary of the influence of Lobdell parameters on characteristic points of the impact response curves (Figure 5).

Model parameter		Maximum force low deflection	Maximum force high deflection	Maximum deflection	Plateau force	Oscillation	Time duration
m_2	figure A.1	+	0	0	0	+	0
m_3	figure A.2	0	+	+	+	0	+
k_{12}	figure A.3	+	0	0	0	+	-
k_{23}	figure A.4	0	+	-	+	0	-
c_{23}	figure A.5-A.6	+	+/-	-	+	-	-

\+ : increase-decrease of value model parameter causes increase-decrease of characteristic point
\- : increase-decrease of value model parameter causes decrease-increase of characteristic point
+/- : increase and decrease of value model parameter causes increase of characteristic point
0 : increase or decrease have minor or no influence

SCALING OF THE RESPONSE REQUIREMENTS

Hamilton et al. [9] determined the ratio of lateral stiffness of a six year old child's thorax by modelling a thorax with finite elements. The calculated stiffness ratio was used to scale the adult lateral thorax response [18] while using Mertz' normalisation and scaling method [8] to obtain the lateral thoracic response of a six year old child. However, Mertz' method ignores the differences in responses due to damping of the internal organs, bony structures and muscular tissues. Regarding the corridors obtained by Kroell et al. [16],[17], it seems that the ratio impactor velocity/impactor mass has a large influence on the force-deflection curve and these large differences can only be caused by internal damping of the thorax [19].

To derive a (scaled) thoracic response of a child with the aid of the simplified Lobdell model, the parameters of the model will be scaled while using scaling procedures for mass, thoracic stiffness and damping. In the previous paragraph it was shown that the effect of the visco-elastic element is small and, therefore, the simplified model will be used instead of the original Lobdell model. This is because of the reduction of the number of the model parameters; besides this the scaling of visco-elastic properties (kv_{23}, cv_{23}) is rather complex and not yet validated. The unknown quantities of the

simplified child thorax Lobdell model are the thorax and spine mass (m_2, m_3), the impactor mass (m_1), the thoracic stiffness (k_{12}, k_{23}) and the thoracic damping (c_{23}). The scaling of these properties is now discussed in detail.

Geometry

The geometry scaling ratios of the thorax are chosen to be:

$$\lambda_x = \frac{\text{chest depth}_{child}}{\text{chest depth}_{adult}}$$
$$\lambda_y = \frac{\text{chest breadth}_{child}}{\text{chest breadth}_{adult}} \quad (1)$$
$$\lambda_z = \frac{\text{chest height}_{child}}{\text{chest height}_{adult}}$$

Thorax mass

The scaling of mass is based on the assumption that the thorax mass is proportional to the thorax volume V while assuming an equal density ρ for child and adult. The volume can be scaled by the geometrical sizes of the thorax:

$$R_m = \frac{\rho_{child} V_{child}}{\rho_{adult} V_{adult}} = \frac{V_{child}}{V_{adult}} = \lambda_x \cdot \lambda_y \cdot \lambda_z \quad (2)$$

Impactor mass

To obtain a similar impact severity, the impactor impulse needs to be scaled. Since the velocity scaling ratio equals one, the impactor mass scales with the same ratio as the thorax mass.

Impactor and sternum stiffness

The differences of the skin and flesh elastic properties for the contact with the impactor due to aging are assumed to be negligible. The spring k_{12} is scaled only by the impactor surface area A_{imp} and the thickness h of skin and flesh between the impactor and the sternum.

$$R_{k\,12} = \frac{k_{12\,child}}{k_{12\,adult}} = \frac{R_A}{R_h}$$
$$R_A = \frac{A_{imp\,child}}{A_{imp\,adult}} = \frac{\text{sternum height} \cdot \text{chest breath}_{child}}{\text{sternum height} \cdot \text{chest breath}_{adult}} = \lambda_z \cdot \lambda_y \quad (3)$$
$$R_h = \frac{h_{child}}{h_{adult}} = \lambda_x$$

Rib cage stiffness

The stiffness of the thorax is modelled by an elastic spring with the parameter k_{23}. The lumped rib cage stiffness depends on the presence of cartilage joints between the ribs and sternum and the ribs and vertebral bodies, the mechanical properties of the cartilage joints and ribs, and the geometrical properties (cross-section and radius) of the ribs. The scaling of the rib cage stiffness parameter k_{23} is based on the differences in cartilage properties, the rib cage curvature and the elastic stiffness properties of the rib itself:

$$R_{k_{23}} = \alpha\,\beta\,\Gamma \quad (4)$$

Here α is the scaling ratio for the differences in cartilage joint stiffness, β is the scaling ratio for the curvature. Γ is the scaling ratio for the elastic properties of the rib itself when the properties captured in the ratios α and β would be invariant. Scaling laws for α, β and Γ will now be derived.

cartilage joint stiffness

The rib cage stiffness ratios are approximated by taking the stiffness ratio of just a single rib of the child and a similar one of the adult. It is assumed that the stiffness ratio of the entire rib cage equals the stiffness ratio of a single rib. The difference in stiffness caused by the anterior cartilage part is scaled by the ratio α and is determined by the ratio of the static stiffness of two curved beams with different boundary conditions. Two extreme boundary conditions are defined: the adult rib is represented by a clamped (fixed) circular beam and the child rib is represented by a simply supported circular beam. The conditions are illustrated in Figure 6. The approximation of the ratios α and β are based on Castigliano's first theorem [20]. The equations are given in annex B of this paper. The support ratio α between a fixed and a simply supported beam is *0.46* and, therefore, the influence of rib connection can be considered large.

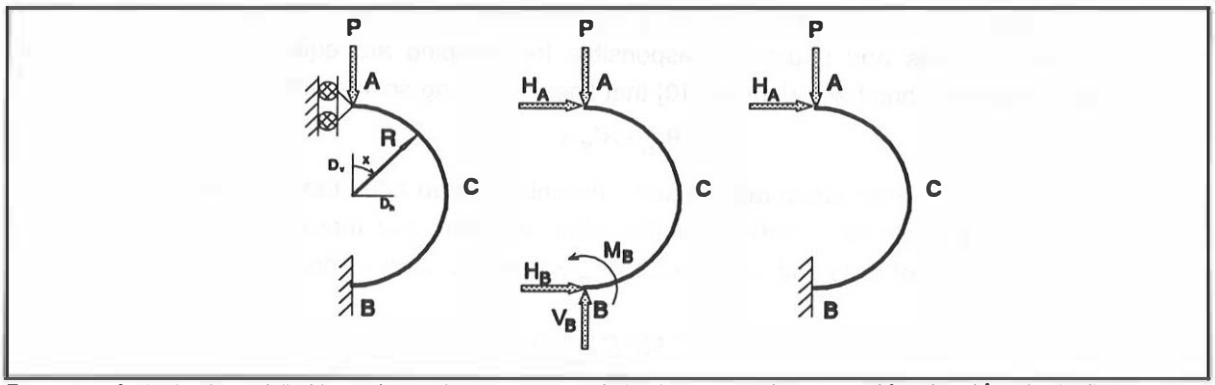

Figure 6 A single rib modelled by a circular beam, upper end simply supported, lower end fixed and free body diagram.

rib curvature

The previous ratio derivation (ratio α) assumes that λ_x is equal to λ_y. The radius of the rib cage can be scaled by one of the cross-sectional parameters; in this case it will be scaled by λ_y. To take into account the different cross-sectional shape, the stiffness scaling factor will be multiplied by the ratio β. This ratio is approximated by comparing the static stiffness of elliptical curved beams of child and adult dimensions. The influence of the curvature is less than *10* percent (β = *1.09*) and, therefore, the influence will be small. More details can be found in annex B.

elastic rib properties

The scaling ratio Γ for the elastic properties of the rib itself is:

$$\Gamma = \frac{\left(\frac{EI}{R^3}\right)_{child}}{\left(\frac{EI}{R^3}\right)_{adult}} = \left(\frac{R_E \cdot R_I}{R_R}\right) \tag{5}$$

$$R_E = \frac{\text{E-modulus, bending}_{child}}{\text{E-modulus, bending}_{adult}}$$

$$R_I = \frac{\text{moment of inertia}_{child}}{\text{moment of inertia}_{adult}}$$

$$R_R = \frac{(\text{radius rib})^3_{child}}{(\text{radius rib})^3_{adult}} = \lambda_y^3$$

The moment of inertia ratio, R_I is approximately *0.09*, R_E=*0.62* and R_R=0.15 for an 18 month old child. More details can be found in annex **B**.

Thorax damping

The thorax damping is caused by the damping of the bony structures, the muscular tissues and the internal organs such as lungs and heart and arteries. It is generally assumed that the damping of the bony structures is negligible [21] and, therefore, the internal organ damping can be qualified as dominant. This was also concluded by Plank and Eppinger [14], who performed a material parameter sensitivity study while using a finite element model to simulate thoracic responses of an adult. They also concluded that the viscosity effects of the muscular tissues were small. This low sensitivity can be explained; Plank and Eppinger modelled the muscles as passive structures with no contact between the muscles and the rib cage. However, visco-elastic properties depend on the rate of muscular activation and active muscles are able to "deform" the rib cage.

As a physiological model of the thoracic damping is not available, a general scaling method was applied for damping. This method holds for linear scaling of the geometry with a factor λ, and for the case where the materials and structures responsible for damping are equal for child and adult. Under these conditions it has been derived [10] that linear damping scales with:

$$R_{c_{23}} = R'_{\sigma} \cdot \lambda \qquad (6)$$

where R'_{σ} is the ratio of stress strain-rate relations for child and an adult thorax. There is no current information on stress strain-rate relations of the adult and the child thorax. Presuming an equal stress strain-rate relation of child and adult thorax, R'_{σ} will be set equal to one.

PREDICTED 18 MONTH OLD CHILD RESPONSE

The child response corridors can be obtained by scaling either the "Kroell thoracic response corridors" or the thoracic impact responses. The scaled Lobdell 18 month old child thoracic response is compared with the scaled "Kroell Thoracic response corridors". Similar to the method used by Hamilton et al. [9], the "Kroell thoracic response corridors" are scaled while using Mertz' normalisation and scaling method, without scaling the damping, while the thoracic responses are scaled by the model-based scaling method, as is presented in this paper.

Mertz' method

The "Kroell thoracic response corridors" have been scaled by Mertz' scaling method for force, time and deflection. The force and deflection scaling ratios are:

$$F_f = \sqrt{R_k R_m} = 0.179$$
$$R_d = \sqrt{\frac{R_m}{R_k}} = 0.780 \qquad (7)$$

where $R_k = R_{k23} = 0.23$ and the thorax and impactor mass will be scaled by $R_m = 0.14$. These ratios are based on the data as shown in Table 4. The child data is obtained from [22] while the material properties are obtained from [23]. The depth and height are obtained from Hamilton [9] by interpolation from a six year old child and a seventy-seven year old female, while using the chest breadth as the interpolation parameter. No values were found on the lower sternum height. The scaled 18 month child "Kroell thoracic response corridors" are shown in Figure 7 by the dotted lines.

Table 4 Scaling parameters and ratios for frontal impact.

Parameter	adult	18 month old child	Ratio	
torso depth axilla	230.0	112.8	λ_x	0.49
torso breadth axilla	305.5	162.2	λ_y	0.53
suprasternal height	590.9	309.1	λ_z	0.52
rib depth	1.48	0.81	γ_x	0.55
rib height	1.48	0.81	γ_z	0.55
rib E-modulus ($kN.mm^{-2}$)	13	8	R_E	0.62
mass	m_{imp} = 19.5; 23.1 m_2 = 0.45 m_3 = 27.2	m_{imp} = 2.7; 3.2 m_2 = 0.063 m_3 = 3.8	R_m	0.14
impactor area (mm^2)	1.8E+4	5.1E+3	R_A	0.28
stiffness skin and flesh ($Kn.m^{-1}$)	281	157	R_{k12}	0.56
rib moment of inertia (mm^4)	-	-	R_I	0.09
damping ($kN.s.m^{-1}$)	compression c_{23} = 0.525 decompression c_{23} = 1.23	compression c_{23} = 0.3 decompression c_{23} = 0.6	R_{c23}	0.50
α	-	-	α	0.46
β	-	-	β	1.09
torso stiffness ($kN.m^{-1}$)	primary k_{23} = 26.3 secondary k_{23} = 78.8 transition point = 31.8 mm	primary k_{23} = 6.05 secondary k_{23} = 18.1 transition point = 15.6 mm	$R_{k23}=R_k$	0.23

The model-based scaling method

The impact response of the 18 month old child was calculated by scaling the simplified Lobdell model masses (m_2 and m_3), sternum stiffness parameter (k_{12}), the rib cage stiffness parameter (k_{23}) and the damping parameter (c_{23}) by equation (2), (3), (3) and (6) respectively while using the data as denoted in Table 4. The scaled model force skeletal-deflection response (v_{imp}=*4.92 m.s*$^{-1}$, m_{imp}= *2.7 kg*) is shown in Figure 7 while using different scaling ratios for damping. The figure indicates a highly overdamped characteristic of the system. The results obtained show that there are large differences between the method of Mertz (scaling mass and elastic properties) and the response scaling method (scaling mass, elastic properties and damping). The figure indicates that the scaled "Kroell thoracic response corridors" can only be met if the damping scaling ratio is *<0.2*.

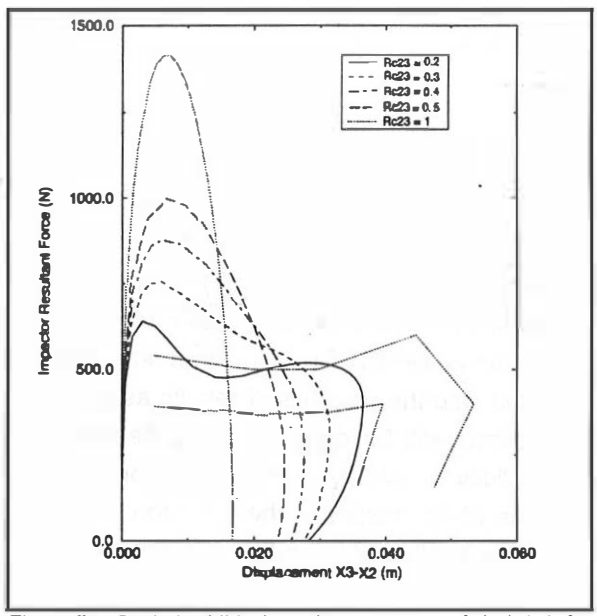

Figure 7 Scaled child thoracic response of Lobdell for different values of R_{c23} and the Mertz' scaled "Kroell thoracic response corridors" (dotted lines).

DISCUSSION AND CONCLUSIONS

In this paper, the "Kroell thoracic response corridors" were scaled using Mertz' method [8] to obtain corridors for an 18 month old child. This is similar to the scaling performed by Hamilton et al. [9] to establish the lateral thoracic response of a six year old child. Scaling the "Kroell thoracic response corridors" however assumes that the child thoracic damping is equivalent to those of adults while the model-based scaling method scales the adult Lobdell model responses, including the thoracic damping. The simulations show that the scaled "Kroell thoracic response corridors" can only be met by the scaled Lobdell response when the damping scaling ratio small (<0.2), which does not seem very realistic.

Besides the dominant damping behaviour (69 percent and 66 percent energy dissipation for the adult and the 18 month child) respectively, the influence of the type of rib support modelled by the joint cartilage stiffness scaling ratio α seems to be an important phenomenon because it reduces the child rib cage stiffness by more than *50* percent. When having the same impact conditions and the same material properties but using different anatomical configurations (rib-connections), the maximal compression of the child sternum relative to the thorax depth is considerably larger than the adult sternum displacement. This is in contrast to the results derived by Plank and Eppinger [14] with their finite element thorax model. The reason for this is that their material properties variations of the cartilage joints were not as extreme as in this study and as in reality. The curved beam model is not yet validated with the response of PMHS or volunteers but the results indicate that the supports/connection between the ribs and the spine or sternum must be modelled accurately while the influence of the difference in adult/child curvature is small.

The following conclusion can be drawn from this and previous studies: thoracic damping is an important phenomenon. Therefore, besides the scaling methods for mass and elastic structures, scaling of damping must be applied to scale a thoracic response. The model-based scaling method presented in this paper is not validated but it is useful to obtain an approximate thoracic response for children. The validity of the predicted thoracic responses will be studied in detail during future research projects.

FUTURE RESEARCH

In the near future the rib cage of an average (50 percentile) adult will be three dimensionally modelled with MADYMO using finite elements (FE) and including internal organs, such as lungs and heart, and active Hill type muscle models [24]. The response of this model will be omni-directionally validated with the normalised results as published in the literature [16],[17],[18]. The response of the child thorax will be obtained using detailed anthropometric data [22] and material properties [10]. The validity of this child model can only be assessed from an impact child thoracic response. In absence of this response the adult to child scaling parameters that will be selected will be based on sensitivity studies with the FE child thorax.

REFERENCES

[1] ECE Regulation 44 (1991): *Uniform Provisions Concerning the Approval of Restraining Devices for Child Occupants of Power-Driven Vehicles (Child Restraint Systems).* United Nations, Geneva-SUI: E/ECE 324, E/ECE/TRANS/505, Including Revisions, Appenda, Amendments and Corrections, Edition April 1991.

[2] Planning Document on Potential Standard 213 Upgrade (1991): *Federal Motor Vehicle Safety Standard, Child Restraint Systems.* NHTSA, Document No. 75-09, Notice 21, 49 CRF Part 521, July 1991.

[3] Beusenberg M.C. (1992): *Results of an Inquiry Concerning Future Child Crash Dummies.* ISO/TC22/SC12/WG5 Document N354, technical report, Delft-NL.

[4] Beusenberg M.C., Happee R., Twisk D. and Janssen E.G. (1993): *Status of Injury Biomechanics for the Development of Child Dummies.* SAE paper **933104**, Proceedings Child Occupant Protection Symposium, 219-241.

[5] Kallieris D., Barz J., Schmidt G., Heess G. and Mattern R. (1976): *Comparison between Child Cadavers and Child Dummy by using Child Restraint Systems in Simulated Collisions.* SAE paper **760815**, Proceedings STAPP Conference, 513-542.

[6] Wismans J., Stalnaker R.K. and Maltha J. (1981): *Comparison Study of Two 3-Year Old Child Dummies in a Harness Type Child Restraint System.* Proceedings VIth International IRCOBI Conference on The Biomechanics of Impacts, 321-330.

[7] Brun Cassan, F., Page, M., Pincemaille, Y., Kallieris, D. and Tarriere, C. (1993): *Comparative Study of Restrained Child Dummies and Cadavers in Experimental Crashes.* SAE paper **933105**, Proceedings Child Occupant Protection, 243-260.

[8] Mertz, H.J. (1984): *A Procedure for Normalizing Impact Response Data.* SAE paper **840884**. Government/Industry Meeting & Exposition, Washington.

[9] Hamilton M.N., Chen H.H. and Guenther D.A. (1986): *Adult to Child Scaling and Normalizing of Lateral Thoracic Impact Data.* SAE paper **861883**, Proceedings STAPP Conference, 143-156.

[10] Happee, R. (1994): *Scaling of response requirements for child dummies.* TNO-report in progress, TNO Crash-Safety Research Centre, Delft NL.

[11] Snyder R.G. et al. (1977): *Anthropometry of Infants, Children and Youths to Age 18 for Product Safety Design.* Report **UM-HSRI-77-17**, University of Michigan, MI-USA.

[12] Chen P. (1973): *Dynamic Response of the Human Thoracic Skeletal System To Chest Impact.* Phd. Thesis, UCLA, Los Angeles.

[13] Hamilton M.N., Chen H.H., Guenther D.A. and Cheng P. (1988): *Computer Simulation of the Child Thorax.* SAE paper **881724**, Proceedings STAPP Conference, 165-184.

[14] Plank G.R. and Eppinger R.H. (1989): *Computed Dynamic Response of the Human Thorax From a Finite Element Model.* Proceedings Twelfth International Technical Conference on Experimental Safety Vehicles, Goteborg, 665-672.

[15] Lobdell, T.E., Kroell, C.K., Schneider, Hering, W.E. and Nahum, A.M. (1973): *Impact Response of the Human Thorax.* Human Impact Response, Plenum Press, New York, 201-245.

[16] Kroell C.K., Schneider, D.C. and Nahum, A.M. (1971): *Impact Tolerance and Response of the Human Thorax.* SAE paper **710851**. Proceedings STAPP Conference, 84-134.

[17] Kroell C.K., Schneider, D.C. and Nahum, A.M. (1974): *Impact Tolerance and Response of the Human Thorax II.* SAE paper **741187**, Proceedings STAPP Conference, 383-457.

[18] Tarrière C., Walfisch G., Fayon A., Rosey J.P., Got A., Patel A. and Delams A. (1979): *Synthesis of Human Tolerances Obtained from Lateral Impact Simulations.* Proceedings Seventh International Technical Conference on Experimental Safety Vehicles, Paris, 359-373.

[19] Neathery R.F. and Lobdell T.E. (1973): *Mechanical Simulation of Human Thorax Under Impact.* SAE paper **730982**, Proceedings STAPP Conference, 451-466.

[20] Roark R.J. and Young W.C. (1975): *Formulas for Stress and Strain.* Fifth Edition, McGraw-Hill Kogakusha Ltd., Tokyo.

[21] Yamada, H. (1970): *Strength of Biological Materials.* Williams and Wilkins, Baltimore, Maryland.

[22] Twisk D. (1993): *Anthropometric Data for Children for the Development of Dummies.* TNO report **750161275-B** and **-C**. TNO Crash-Safety Research Centre, Delft NL.

[23] Happee R. (1993): *Injury Biomechanics of Children. A literature Survey on Material Properties and Overall Organism Response and Tolerances.* Internal TNO-report **751310196**, TNO Crash Safety Research Centre, Delft NL.

[24] Happee R. and Thunnissen J.G.M. (1994): *The Role of Muscular Dynamics in Impact Conditions, Simulation of Head/Neck Behaviour In Frontal Car Crashes.* Second World Congress on Biomechanics, Amsterdam NL.

Annex A The parameter sensitivity of the Lobdell model

A sensitivity analysis using a Lobdell model implemented in MADYMO was conducted in order to observe the influence of each model parameter on the impact response. In the current analysis, the 1971 Kroell PMHS initial impactor tests conditions [16] were used (Table 1). The "Kroell thoracic response corridors", a bounded area to which the response of the model is restricted, will be used as performance requirement of the model.
The permutations are performed for both impactor conditions, however for presentation reasons, the figures shown in this section only show the permutations from the low velocity impact condition.
Increasing the mass m_2 causes a phenomenon called backfiring, because the thorax system becomes overdamped, Figure A.1. The mass m_2 affects the whole response whereas the mass m_3 mainly affects the high deflection part of the force-deflection curve as illustrated in Figure A.2. The influence of the rib stiffness factor k_{12} and the internal organ stiffness factor k_{23} is illustrated by Figure A.3 and Figure A.4 respectively.

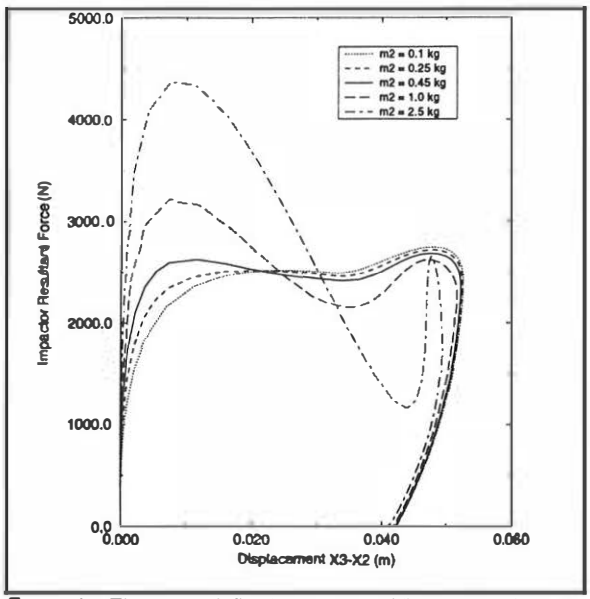

Figure A.1 The force-deflection curves while permutating m2.

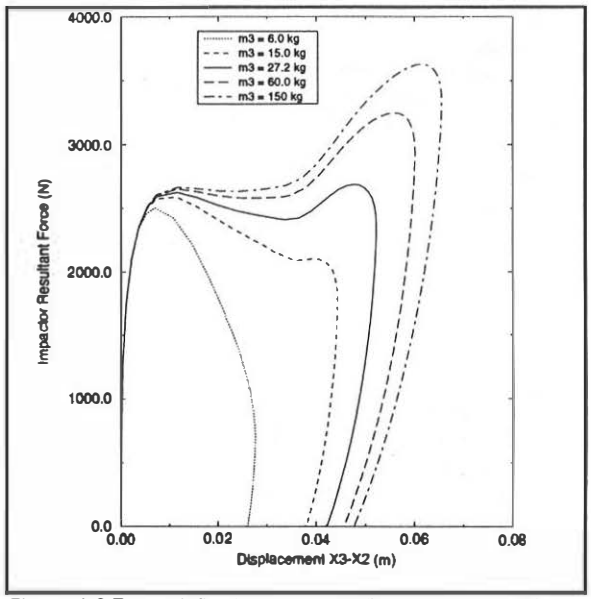

Figure A.2 Force-deflection curves while permutating m3.

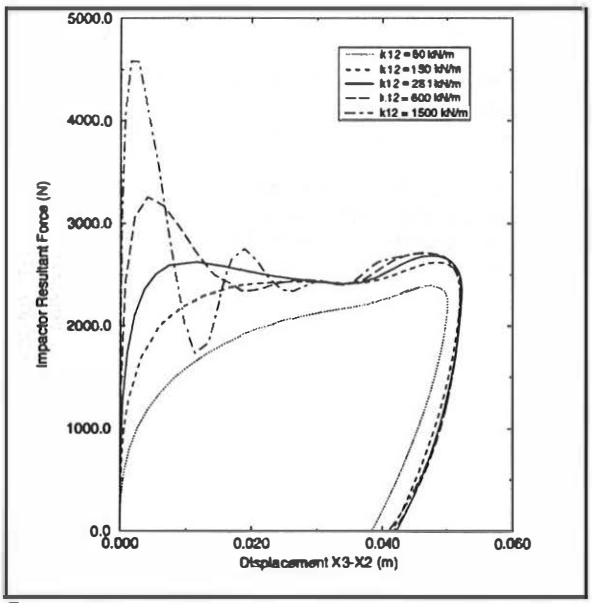

Figure A.3 Force-deflection curves while permutating k12.

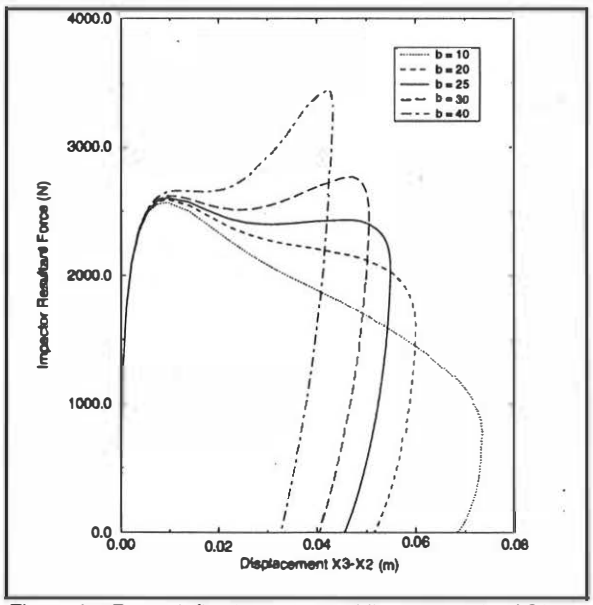

Figure A.4 Force-deflection curves while permutating k23.

Varying the value of k_{23} is done by replacing the bi-linear spring with an approximately corresponding exponential function:

$$F(\Delta X) = a(e^{b\Delta X} - 1) \qquad (A.1)$$
$$a = 700 \ , \ b = 25$$

In the sensitivity analysis the parameter b is permutated.
The influence of the damping factor is large, as illustrated in Figure A.5 and Figure A.6 for compression and decompression respectively. The figures illustrate how the model can tuned with these damping parameters.

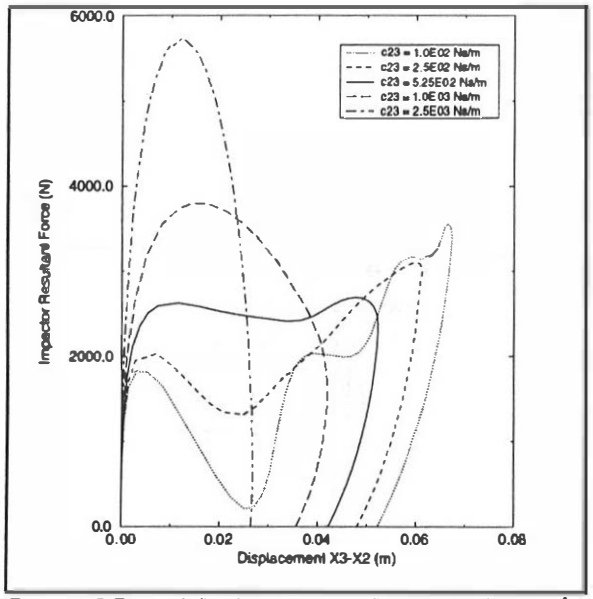

Figure A.5 Force-deflection curves while permutating c_{23} for compression.

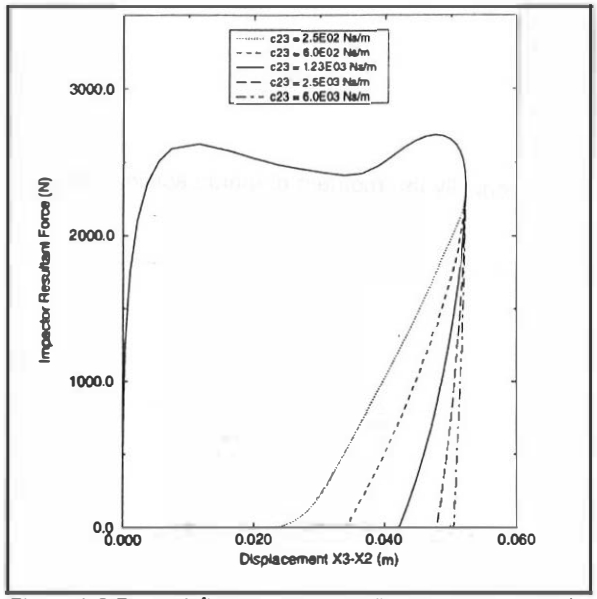

Figure A.6 Force-deflection curves while permutating c_{23} for decompression.

The influence of cartilage joints

Having flexible cartilage joints between the ribs and the spine (instead of a rigid connection) reduces the overall rib cage stiffness. This reduces the non-linear spring k_{23} by *50* percent. The influence of this reduction is shown in Figure A.7 by the solid line (compare with the solid lines in figure A6). Figure A.7 also denotes the influence of different damping coefficients c_{23}. It seems that the original "Kroell thoracic response corridors" cannot be met by changing the damping coefficient. This illustrates that the choice of Lobdell model parameters is unique and that the dampIng coefficient c_{23} is a realistic representation of the internal damping and does not incorporate an unrecognized part of the elastic (static) rib cage stiffness. The internal damping dissipates 69 percent of the total impact energy.

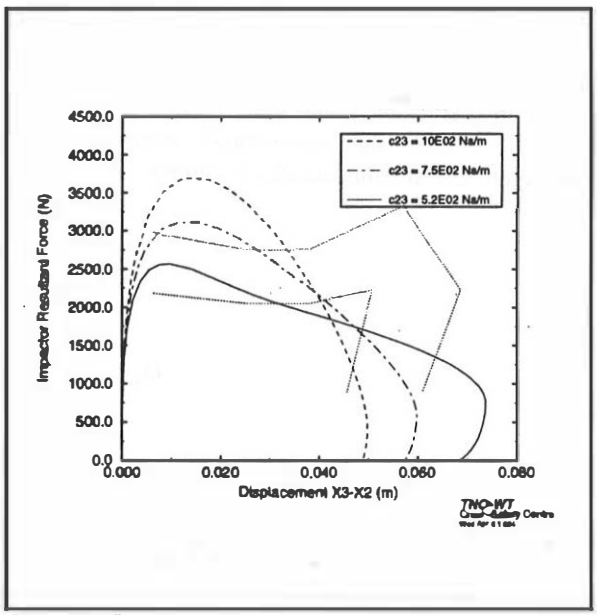

Figure A.7 The Lobdell responses while the rib cage stiffness is reduced by 50 percent and permutating the internal damping coefficient c_{23}.

Annex B Scaling of the rib cage stiffness

Moment of inertia ratio

To derive a scaling ratio for the moment of inertia of the rib an elliptical cross-section is assumed as shown in Figure B.1. The moment of inertia for an elliptical cross-section equals:

$$I_z = \frac{\pi}{4} ab^3 \tag{B.1}$$

The geometric scaling ratios of the rib are chosen to be:

$$\gamma_x = \frac{b_{child}}{b_{adult}} \qquad \gamma_z = \frac{a_{child}}{a_{adult}} \tag{B.2}$$

Subsequentially the moment of inertia scaling ratio is:

$$R_{I_z} = \gamma_x^3 \cdot \gamma_z \tag{B.3}$$

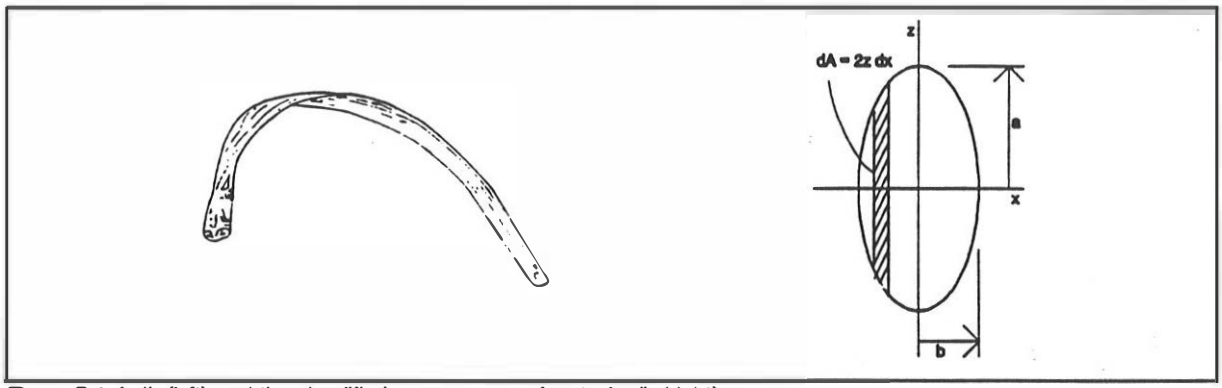

Figure B.1 A rib (left) and the simplified cross-section of a single rib (right).

Cartilage joint stiffness ratio

First the influence of the cartilage joint stiffness denoted by the factor α, is approximated. The derivation is based on Castigliano's first theorem and stiffness will be calculated using $F=kD_v$. The loaded rib, as shown in Figure 6, is statically undetermined. However, the reaction forces can be determined from the equations of equilibrium and one known displacement:

$$\begin{aligned} \textstyle\sum F_H = 0 &\Rightarrow H_A + H_B = 0 \\ \textstyle\sum F_V = 0 &\Rightarrow V_B = P \\ \textstyle\sum M_B = 0 &\Rightarrow M_B = H_A 2R \end{aligned} \tag{B.4}$$

$$M_x = -PR\sin x + HR\cos x \;;\; \frac{\partial U_f}{\partial H} = 0 \tag{B.5}$$

$$\frac{\partial U_f}{\partial H} = \frac{1}{EI}\int_0^{\pi}[HR(1-\cos x)-PR\sin x]R(1-\cos x)R\,dx = \frac{R^3}{EI}\int_0^{\pi}[H(1-2\cos x+\cos^2 x)-P(\sin x-\sin x\cos x)]dx$$

$$= \left[H\left(\frac{3}{2}x-2\sin x+\frac{1}{4}\sin 2x\right)-P\left(-\cos x+\frac{1}{2}\cos^2 x\right)\right]_0^{\pi} \Rightarrow \frac{3\pi}{2}H = 2P \Leftrightarrow H = \frac{4}{3\pi}P \tag{B.6}$$

$$M(x) = \frac{4}{3\pi}PR(1-\cos x)-PR\sin x \tag{B.7}$$

$$\frac{\partial U}{\partial V} = \frac{1}{EI}\int_0^{\pi}\left[\frac{4}{3\pi}PR(1-\cos x)-PR\sin x\right]R\sin x R\,dx = \frac{PR^3}{EI}\int_0^{\pi}\left[\frac{4}{3\pi}(\sin x-\cos x\sin x)-\left(\frac{1}{2}-\frac{1}{2}\cos 2x\right)\right]dx$$

$$= \frac{PR^3}{EI}\left[\frac{4}{3\pi}\left(-\cos x+\frac{1}{2}\cos^2 x\right)-\left(\frac{1}{2}x-\frac{1}{4}\sin 2x\right)\right]_0^{\pi} = \frac{PR^3}{EI}\left[\frac{8}{3\pi}-\frac{\pi}{2}\right] = -0.722\frac{PR^3}{EI} \tag{B.8}$$

Using the equation $F=kD_v$, the adult rib cage stiffness becomes:

$$k_{adult} = 1.39 \frac{EI}{R^3} \tag{B.9}$$

The child rib cage stiffness is obtained, with a thorax radius of 0.0811 m, Table 4:

$$k_{child} = 0.637 \frac{EI}{R^3} \tag{B.10}$$

This leads to a cartilage stiffness ratio:

$$R_k = \frac{k_{child}}{k_{adult}} = \alpha \frac{\left(\frac{EI}{R^3}\right)_{child}}{\left(\frac{EI}{R^3}\right)_{adult}} \quad ; \quad \alpha = 0.46 \tag{B.11}$$

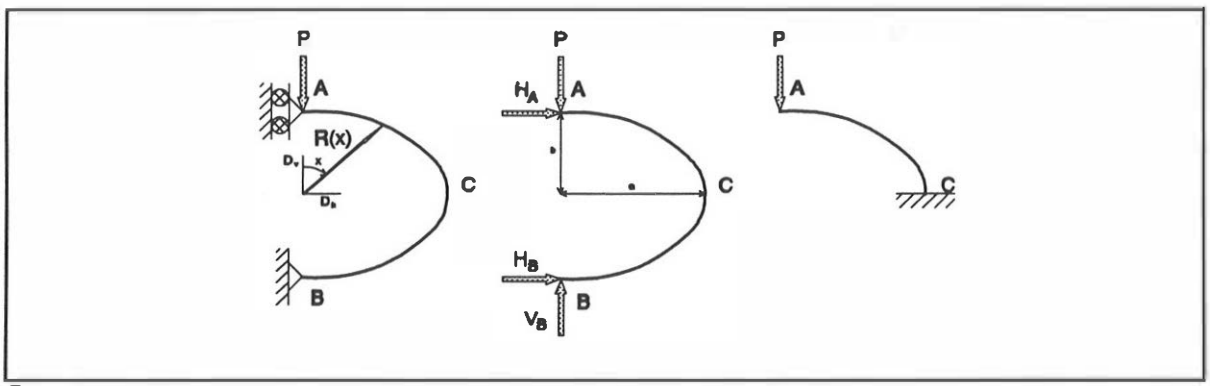

Figure B.2 Single rib modelled by an elliptical beam, both ends simply supported and free body diagram.

Curvature stiffness ratio

The curvature stiffness ratio (β), which takes into account the different elliptical cross-sections, is approximated in this paragraph (see Figure B2). The approximation is also based on Castigliano's theorem and stiffness will be approximated by using $F=kD_v$. The reaction forces can be obtained from equations (B.4) if the stiffness ratio is determined directly from equation:

$$R(x) = \frac{ab}{\sqrt{b^2\sin^2 x + a^2\cos^2 x}} \quad ; \quad M(x) = -PR(x)\sin x$$

$$U_f = 2\int_0^{\frac{\pi}{2}} \frac{[PR(x)\sin x]^2 R(x)dx}{2EI} \quad ; \quad D_v = \frac{\partial U_f}{\partial V} = -\frac{\partial U_f}{\partial P} = -\frac{2P}{EI}\int_0^{\frac{\pi}{2}} R^3(x)\sin^2 x dx \tag{B.12}$$

The radius of the rib cage will be scaled twice, see also equation (B.11). In order to exclude the radius of the elliptical beam, the stiffness of the elliptical beam of the adult must be divided by the stiffness of the elliptical beam of the adult with adapted child dimensions. Since the radius is scaled by λ_y, the y-direction (lateral) parameter a must be kept constant the x-direction (A-P) parameter b will be adapted. The stiffness of the adult and the adapted adult is obtained by numerically solving equation (B.12) and using $F=KD_v$. The associated parameters are presented in Table B.1 and the resulting curvature ratio β for an 18 month child is 1.09.

Table B.1 Difference in rib curvature and the related rib cage stiffness for child, adapted child and adult.

	y-direction a [m]	x-direction b [m]	k_{ell}
Child	8.11E-02	5.64E-02	0.31
Child adapted	1.53E-01	1.06E-01	2.3
Adult	1.53E-01	1.16E-01	2.3